Nanoscale

COMMUNICATION

View Article Online
View Journal | View Issue

Controlled formation of GeSi nanostructures on periodic Si (001) sub-micro pillars

Cite this: *Nanoscale*, 2014, **6**, 3925

Received 7th August 2013
Accepted 13th October 2013

DOI: 10.1039/c3nr04146h

www.rsc.org/nanoscale

Tong Zhou,[a] Cheng Zeng,[b] Qianqian Ma,[a] Yingjie Ma,[a] Yongliang Fan,[a] Zuimin Jiang,[a] Jinsong Xia*[b] and Zhenyang Zhong*[a]

Self-assembled GeSi nanostructures on periodic Si (001) sub-micro pillars (SMPs) are systematically studied. Different GeSi nanostructures, including circularly arranged quantum dots, quantum rings and quantum dot molecules can be readily obtained at the edge of the pillars by controlling the growth temperatures and the diameter of the pillar. These phenomena are explained by taking into account the surface chemical potential around the top terrace of SMPs, which is considerably affected by the formation of {113} facets. Our results demonstrate a feasible route to obtain novel periodic Si pillars embedded with the desired GeSi nanostructures, which have promising applications in optoelectronic devices.

Semiconductor quantum nanostructures (QNs) have been of great interest for their promising applications in optoelectronic devices, such as single photon sources, light-emitting diodes, and infrared photodetectors.[1–3] In particular, GeSi QNs have been widely studied due to their compatibility with sophisticated Si technology.[4] Although the quantum efficiency of Ge/Si systems is quite poor owing to the indirect band gap, enormous effort has still been devoted to explore the GeSi QNs on flat Si (001) substrates for their optoelectronic applications,[5,6] because the law of momentum conservation can be relaxed by breaking the crystal symmetry or by phonon localization in nanostructures.[7] Recently, microcavities, such as Fabry–Perot microcavities, photonic crystal (PhC) microcavities, and whispering gallery microcavities (WGM), have been widely exploited to manipulate the light emission of QNs.[8–11] The quantum efficiency of GeSi QNs can be improved by embedding them into pillars,[12–14] which are regarded to be an optical WGM.[15] The resonant modes of WGM are located in close proximity to the sidewalls of pillars. If the GeSi QNs are embedded there, and the spontaneous emission of the QNs matches with the resonant mode of WGM, the strong light-matter coupling phenomena, such as resonant radiation and Purcell effect, are expected in the QNs. Moreover, in the case of laterally periodic pillars acting as a two-dimensional PhC, the extraction and collection efficiency of the emission in the vertical direction can be remarkably enhanced through the redistribution of the energy to the vertical mode due to the effect of PhC band gap.[16] Accordingly, the periodic pillars embedded with QNs in proximity to the sidewalls can have both improved quantum efficiency and increased extraction efficiency of the emission in the vertical direction. However, the fabrication and the characterization of such structures have rarely been studied in detail.

In this letter, we report on controlled GeSi QNs on periodic Si (001) sub-micro pillars (SMPs). By controlling the growth conditions and the diameters of the SMPs, different GeSi QNs, including circularly arranged quantum dots (QDs), quantum rings (QRs), and quantum dot molecules (QDMs), are realized at the edge of SMPs. Such preferential growth of GeSi QNs is explained in terms of the surface chemical potential and the anisotropic surface diffusion of adatom around the top terrace edge of SMPs. We find that the surface chemical potential is considerably affected by the formation of {113} facets, which is associated with the diameter and the growth conditions. By designing the diameter and the period of the SMPs, the strong coupling between spontaneous emission of GeSi QNs and the whispering gallery modes of SMP and the effect of the PhC bandgap both improve the light emission of GeSi QNs, which have promising future in the application of optoelectronic devices.

The samples are grown on prepatterned Si (001) substrates with two-dimensionally (2D) ordered silicon SMPs by molecular beam epitaxy. The 2D ordered SMPs are perpendicular to the Si (001) substrates with a flat and circular (001) top terrace, which are obtained by electron beam lithography and inductive coupled plasma etching. The period, diameter and height of SMPs are intentionally controlled. The SMP with a period T and a diameter D is denoted by P_T^D. All substrates are cleaned using

[a]*State Key Laboratory of Surface Physics, Key Laboratory of Micro and Nano Photonic Structures (Ministry of Education) and Department of Physics, Fudan University, Shanghai 200433, China. E-mail: zhenyangz@fudan.edu.cn; Fax: +86-21-65643278; Tel: +86-21-65643278*

[b]*Wuhan National Laboratory for Optoelectronics, Huazhong University of Science and Technology, Wuhan 430074, China. E-mail: jinsongxia@gmial.com*

the RCA method followed by HF treatment to form a hydrogen-terminated surface before loading into the growth chamber. After the thermal desorption of the hydrogen at 800 °C for 3 min, a Si buffer layer of 50 nm was grown at a growth rate of 0.6 Å s^{-1} while ramping the temperature from 430 °C to 480 °C. Subsequently, 10 monolayer (ML) Ge is deposited at a growth rate of 0.05 Å s^{-1} at 500–580 °C. The surface morphologies of the samples are characterized using atomic force microcopy (AFM) (Veeco DI Multimode V SPM) in tapping mode.

Fig. 1(a) and (b) show the AFM images of samples with SMPs of p_{600}^{550} and p_{400}^{350} after 50 nm Si buffer growth, respectively. We find that the surface morphology is not so much different due to the relatively low growth temperature. The main variation of the SMPs after buffer layer growth is the decrease of the diameter gradually toward the top, as demonstrated in the cross-sectional height profiles in Fig. 1(c) and (d). In addition, for SMPs with large diameter, *e.g.* p_{600}^{550}, the former flat top terrace evolves to a plate-like one with a central basement of a relative depth of about 3.5 nm. The width of the 'plate' edge is about 178 nm. We also find a similar plate-like surface with an edge width of ~172 nm on the top of SMPs of p_{600}^{450} (not shown).

Fig. 2(a)–(c) shows the surface morphologies of samples with SMPs of p_{600}^{550} after 10 ML Ge deposition at 500, 540 and 580 °C, respectively. It can be seen that different GeSi nanostructures are obtained at different temperatures. For Ge growth at 500 °C, the former plate-like top terrace of SMPs essentially remained except that the depth and the edge width of "plate" become 5.1 nm and 192 nm, respectively. In addition, some small mounds, indicated by a white arrow in Fig. 2(a), appear at the edge of the SMPs. For Ge growth at 540 °C, the former plate-like top terrace of SMPs disappears. Instead, GeSi nanoislands appear at the edge of the flat top terrace of SMPs, which form circular necklaces of nanoislands on the top of SMPs. The height of nanoislands is 3.5 ± 1 nm. We find that the nanoislands are still bound by {105} facets. The asymmetrical shape of nanoislands is attributed to the local substrate vicinity.[17] When the growth temperature of Ge increases further to 580 °C, GeSi QRs with the diameters of about 300 nm and the heights of 8.0 ± 0.5 nm are clearly seen at the edge of the top flat terrace of SMPs, as shown in Fig. 2(c).

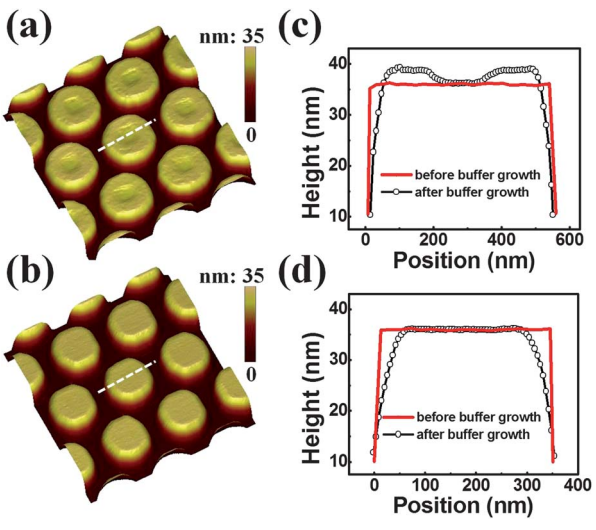

Fig. 1 AFM images of SMPs of (a) p_{600}^{550} and (b) p_{400}^{350}, after 50 nm Si buffer growth, the height profiles across the center of SMPs of (c) p_{600}^{550} and (d) p_{400}^{350}, before and after Si buffer growth. The white dashed lines in (a) and (b) denote the position of the height profiles in (c) and (d) respectively.

Furthermore, we find that the evolution of the self-assembled GeSi QNs also depends on the diameter of the SMPs. Fig. 3(a) and (b) show the surface morphologies of samples with SMPs of p_{600}^{450} and p_{450}^{350} after 10 ML Ge deposition at 580 °C. On SMPs of p_{600}^{450}, QDMs are obtained, which are composed of four small hut-like QDs at the edge of the top terrace of the SMPs. The QDs of QDMs have heights of 13.3 ± 0.9 nm and sidewalls of {105} facets. On SMPs of p_{450}^{350}, big dome-like QDs are obtained on the center of the top terrace of the SMP, whose sidewalls are dominant with {113}, {105}, and (001) facets. Comparing Fig. 2(c) and Fig. 3, it is evident that different QNs of QRs, QDMs and QDs are obtained on SMPs with different diameters.

It is well known that the diffusion of adatoms is controlled by the surface chemical potential, which is related to the curvature and the strain field on the surface. In general, the surface chemical potential is given by,[18,19]

$$\mu = \mu_0 + \Omega\gamma\kappa + \Omega E_S \quad (1)$$

where μ_0 is the chemical potential of flat surface, Ω is the atomic volume, γ is the surface energy per unit area, κ is the surface curvature, E_s is the local strain-relaxation energy. Based on the height profiles, Z, obtained from the AFM data, the sectional surface curvature κ can be obtained by,[18,19]

$$\kappa = -Z''\left[1 + (Z')^2\right]^{-3/2} \quad (2)$$

where Z' and Z'' are the first and second derivatives of Z with respect to the positions. For a given 2D point $Z(x, y)$, the surface curvature $\kappa(x, y)$ is the average of the two principal sectional curvatures obtained from eqn (2).[19] The local strain-relaxation energy E_S is given by,[18,19]

$$E_S = -\frac{C}{2}\left(\frac{\kappa}{|\kappa|}[\kappa(Z_S - Z_0)]^2 - \varepsilon^2\right) \quad (3)$$

where Z_S is the position of the top terrace and Z_0 is the position of the Ge film. The atomic volumes of Si and Ge are 12.1 and 13.6 cm^3 mol^{-1}, respectively. The surface energy and the elastic constant of the Ge layer are 1.835 J m^{-2} and 1.03 × 10^{11} N m^{-2}, respectively.[19] The misfit strain is 0.04.

Fig. 4 shows the surface chemical potential and the corresponding height profile across the center of a SMP of p_{600}^{550}. We find that the surface chemical potential is considerably affected by the Ge thickness denoted by (Z_s − Z_0). For Si buffer layer growth on Si SMPs, the surface chemical potential is only determined by the surface curvature of the SMPs. So there is a local maximum surface chemical potential at the edge of the top terrace of SMPs, as in the case of (Z_s − Z_0 = 0) in Fig. 4. Accordingly, the Si adatoms on the top terrace of SMPs will diffuse from the edge (regions of high chemical potential) toward the centre and the regions between SMPs (regions of low

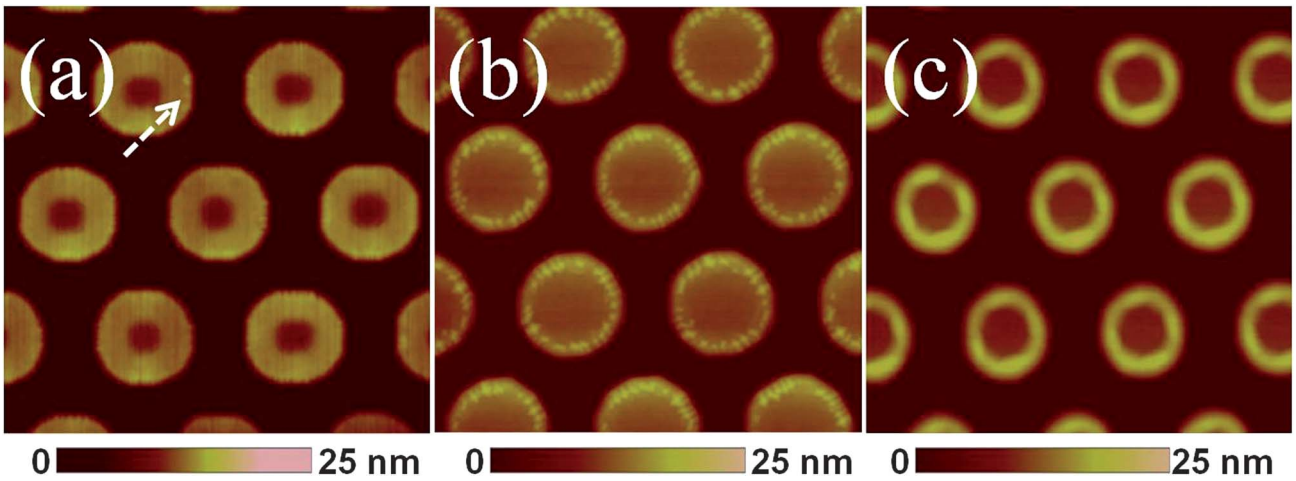

Fig. 2 AFM images of the surface morphologies after 10 ML Ge deposition on SMPs of p_{600}^{550} at (a) 500 °C, (b) 540 °C, and (C) 580 °C. The arrow in (a) indicates a small QD.

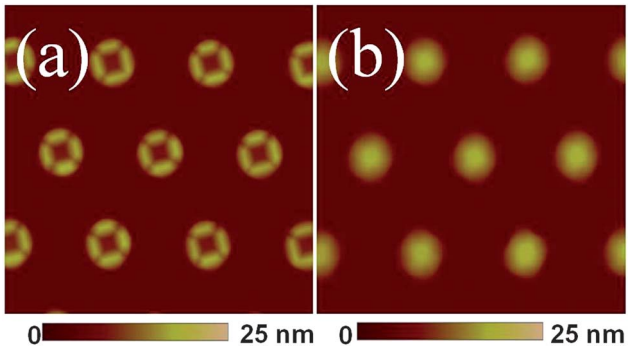

Fig. 3 AFM images of the surface morphologies of SMPs of (a) p_{600}^{450} and (b) p_{450}^{350}, after 10 ML Ge deposition at 580 °C.

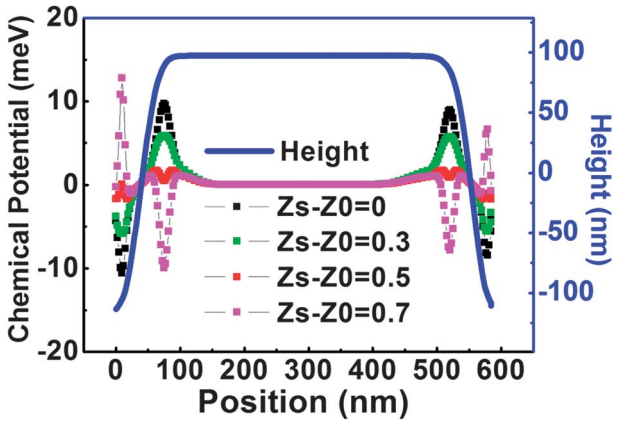

Fig. 4 The surface chemical potential with different thicknesses of the Ge layer denoted by $Z_s - Z_0$ and the corresponding height profile across the center of a SMP of p_{600}^{550}.

chemical potential). As a result, the growth rate at the edge of the top terrace of SMPs is smaller than those on other regions, which leads to the observed decrease of the diameter of the top terrace of SMPs during Si buffer layer growth. In addition, we estimate the surface diffusion length of Si adatoms on the top terrace, which can be given by[20]

$$L = (D\tau)^{1/2},\ D = a^2 \upsilon \exp(-E/k_B T) \quad (4)$$

where D denotes the diffusion constant, τ is the time interval for adatom diffusion, a is the lateral motion corresponding to each hop of the adatom, υ is a prefactor, k_B is the Boltzmann constant, T is the growth temperature, and E denotes the diffusion barrier for the Si adatoms. The calculated diffusion length of Si adatoms is about 190 nm, which is very close to the width of the 'plate' edge mentioned above. Therefore, for SMPs with large diameters, *e.g.* p_{600}^{550}, the migration length of Si adatoms is smaller than the radius of the SMPs on the top terrace at the low growth temperature. Such a kinetically limited diffusion of adatoms result in the plate-like surface on the top of SMPs of p_{600}^{550}, as shown in Fig. 1(a). For SMPs with small diameters, *e.g.* p_{450}^{350}, the top terrace is essentially flat due to the smaller radius than the migration length of adatoms on the top terrace.

Following the Si buffer growth, Ge is deposited. In the case of SMPs of p_{600}^{550}, at low growth temperatures, *e.g.* 500 °C, the surface morphology after Ge growth is only slightly changed due to the limited diffusion length of Ge adatoms. Therefore, a plate-like top terrace is still observed on SMPs of p_{600}^{550}, as shown in Fig. 2(a). At high growth temperatures, the Ge growth is affected by the surface chemical potential, which is a result of the competition between the surface energy and the strain energy. At the beginning of the Ge growth, the surface energy still plays the dominant role in the chemical potential, which results in a local maximum of surface chemical potential at the edge of the top terrace of SMPs as in the case of $(Z_s - Z_0 = 0.3)$ in Fig. 4. Accordingly, Ge adatoms preferentially diffuse towards the center from the edge of the top terrace of SMPs. In addition, the surface diffusion length of Ge adatoms is much larger than that of Si ones due to the lower activation energy.[21] As a result, the former concaved region at the center of the top terrace of SMPs of p_{600}^{550} can be filled. With the growth of Ge, the strain energy gradually dominates the surface chemical potential. A

local minimum surface chemical potential gradually appears at the edge of the top terrace of SMPs, as in the case of ($Z_s - Z_0 =$ 0.5 and 0.7) in Fig. 4. The Ge adatoms on the top terrace will then diffuse towards the edge and incorporate there. With further Ge growth, nucleation of Ge nanostructures occurs at the edge of the top terrace, where the critical volume for the nucleation is readily obtained. For SMPs with large diameters, *e.g.* for p_{600}^{550}, small islands are preferentially grown at the edge of the top terrace to form necklaces of nanoislands at a mediate temperature due to the limited diffusion length of Ge atoms, as shown in Fig. 2(b). At high growth temperature, *e.g.* of 580 °C, bigger Ge islands are readily formed at the edge of the top terrace since more Ge atoms incorporates into islands. The coalescence of these bigger islands readily forms Ge nanorings at the edge of the top terrace, as shown in Fig. 2(c).

Moreover, in the case of SMPs of p_{600}^{450} and p_{450}^{350}, the {113} facets appear near the top terrace of SMPs after 10 ML Ge growth at low temperature of 500 °C, as denoted by the yellow dashed lines in Fig. 5(b) and (c). Such a formation of {113} facets is energetically driven,[22] which is associated with the surface energy and the surface area of {113} facets. The smaller the pillars, the larger the {113} facets. Accordingly, there are essentially no {113} facets observed on SMPs of p_{600}^{550}, as shown in Fig. 5(a). These surface morphologies of SMPs can be regarded as those of the wetting layer prior to the formation of GeSi QNs. The corresponding 2D surface chemical potentials are calculated and shown in Fig. 5(d)–(f) for SMPs of p_{600}^{550}, p_{600}^{450} and p_{450}^{350}, whose surface morphologies are shown in Fig. 5(a)–(c), respectively. For chemical potential of SMPs with large diameter, *e.g.* p_{600}^{550}, a ring-like potential minimum appear at the edge of the top terrace of SMPs, as denoted by two black dashed circles in Fig. 5(d). Thus, depending on the growth conditions, necklace of QDs or QRs can be obtained on p_{600}^{550}, as shown in Fig. 2(b) and (c). Whereas the formation of {113} facets considerably affect the surface chemical potential because the edges between {113} facets and the top terrace have a relatively smaller curvature than others. Therefore, the surface chemical potential minimum at the edge of the top terrace of SMPs with {113} facets does not continue. For SMPs of p_{600}^{450} with {113} facets of small area, fourfold stripes of local potential minima appear at the edge of the top terrace, as denoted by the black dashed line contours in Fig. 5(e). The preferential growth of Ge in those regions with local potential minima results in the QDMs, as shown in Fig. 3(a). For SMPs of p_{450}^{350} with {113} facets of large area, four small dots of local potential minima appear at the corners of the top terrace formed by the {113} facets and the top terrace, as denoted by the small black dashed circles in Fig. 5(f). Although the Ge also preferentially grows in those corners, Ge QNs are not formed there due to the quite small region and the efficient strain relaxation on the convex corners. Considering the efficient strain relaxation due to the small diameter of p_{450}^{350}, only one big dome-like island is obtained on the top, as shown in Fig. 3(b).

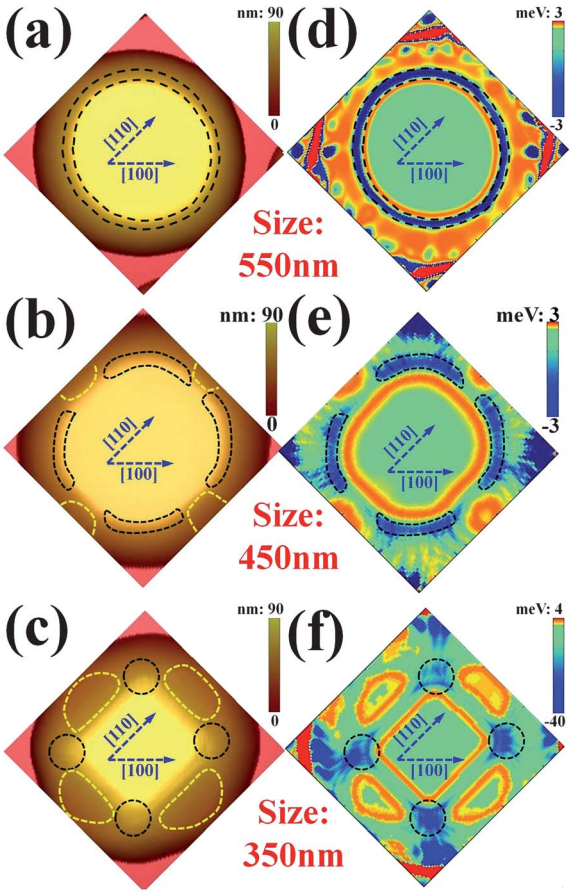

Fig. 5 3D AFM images of a SMP of (a) p_{600}^{550}, (b) p_{600}^{450}, and (c) p_{450}^{350}, after 10 ML Ge growth at 500 °C, (d)–(f) are the corresponding 2D surface chemical potentials. The black dashed line contours indicate the regions of local chemical potential minima. The yellow dashed line contours in (b) and (c) denote the regions of {113} facets. The fitting parameter ($Z_s - Z_0$) is 0.5 nm.

The Si SMPs embedded with Ge QNs can have unique properties. The spontaneous emission will be enhanced due to the Purcell effect when it is coupled with the whispering-gallery mode. Thanks to the sidewalls of the SMPs, more photons can escape from the silicon. By designing the diameter and the period of the SMPs, the optical confinement and the enhancement of the extraction of emission by the PhC can be realized. In addition, the coupled QDMs (as shown in Fig. 3(a)) may have potential applications in quantum computation devices based on quantum cellular automata.[23]

In summary, self-assembled GeSi QNs on 2D hexagonally ordered silicon SMPs are systematically studied. Well-controlled GeSi QNs, including necklace of QDs, QRs and QDMs, are obtained at the edge of the SMPs by controlling the growth conditions and the surface morphology of SMPs. These results are explained in terms of the surface chemical potential around the top of the SMPs, which is considerably affected by the formation of {113} facets. The novel structures of the QNs-cavity system may have promising applications in optoelectronic devices. Our results of controlled formation of QNs should be also adaptable for other heteroepitaxial growth, such as InAs/GaAs systems.

Acknowledgements

This work was supported by the special funds for the Major State Basic Research Project (no. 2009CB929300,

2011CB925601, 2013CB632104, and 2013CB933303) of China, and the Natural Science Foundation of China (NSFC) under Project no. 10974031 and 61177049, and the Ph.D Programs Foundation of Ministry of Education of China (grant 20110142120059). Tong Zhou also thanks the support from Fudan University by the Research Support Project for Outstanding Ph.D Students. We thank the engineers in the Center of Micro-Fabrication and Characterization (CMFC) of WNLO for the support in the electron beam lithography.

Notes and references

1 P. Michler, A. Imamoglu, M. D. Mason, P. J. Carson, G. F. Strouse and S. K. Buratto, *Nature*, 2000, **406**, 968.
2 Q. Sun, Y. A. Wang, L. S. Li, D. Wang, T. Zhu, J. Xu, C. Yang and Y. Li, *Nat. Photonics*, 2007, **1**, 717.
3 S. Tong, J. L. Liu, J. Wan and K. L. Wang, *Appl. Phys. Lett.*, 2002, **80**, 1189.
4 K. L. Wang, D. Cha, J. Liu and C. Chen, *Proc. IEEE*, 2007, **95**, 1866.
5 M. W. Dashiell, U. Denker and O. G. Schmidt, *Appl. Phys. Lett.*, 2001, **79**, 2261.
6 J. Wan, G. L. Jin, Z. M. Jiang, Y. H. Luo, J. L. Liu and K. L. Wang, *Appl. Phys. Lett.*, 2001, **78**, 1763.
7 D. Liang and J. E. Bowers, *Nat. Photonics*, 2010, **4**, 511.
8 K. J. Vahala, *Nature*, 2003, **424**, 839.
9 C. Brüggemann, A. V. Akimov, A. V. Scherbakov, M. Bombeck, C. Schneider, S. Höfling, A. Forchel, D. R. Yakovlev and M. Bayer, *Nat. Photonics*, 2012, **6**, 30.
10 J. S. Xia, Y. Ikegami, Y. Shiraki, N. Usami and Y. Nakata, *Appl. Phys. Lett.*, 2006, **89**, 201102.
11 S. L. McCall, A. F. J. Levi, R. E. Slusher, S. J. Pearton and R. A. Logan, *Appl. Phys. Lett.*, 1992, **60**, 289.
12 J. M. Gérard, D. Barrier, J. Y. Marzin, R. Kuszelewicz, L. Manin, E. Costard, V. Thierry-Mieg and T. Rivera, *Appl. Phys. Lett.*, 1996, **69**, 449.
13 J. M. Gérard, B. Sermage, B. Gayral, B. Legrand, E. Costard and V. Thierry-Mieg, *Phys. Rev. Lett.*, 1998, **81**, 1110.
14 M. Pelton, C. Santori, J. Vučković, B. Zhang and G. S. Solomon, *Phys. Rev. Lett.*, 2002, **89**, 233602.
15 V. N. Astratov, S. Yang, S. Lam, B. D. Jones, D. Sanvitto, D. M. Whittaker, A. M. Fox, M. S. Skolnick, A. Tahraoui, P. W. Fry and M. Hopkinson, *Appl. Phys. Lett.*, 2007, **91**, 071115.
16 S. Noda, M. Fujita and T. Asano, *Nat. Photonics*, 2007, **1**, 449.
17 B. J. Spencer and J. Tersoff, *Appl. Phys. Lett.*, 2010, **96**, 073114.
18 B. Yang, F. Liu and M. G. Lagally, *Phys. Rev. Lett.*, 2004, **92**, 025502.
19 H. Chen, C. Kuan, Y. Suen, G. Luo, Y. Lai, F. Wang and S. chen, *Nanotechnology*, 2012, **23**, 015303.
20 Z. Zhong, A. Halilovic, M. Mühlberger, F. Schäffler and G. Bauer, *J. Appl. Phys.*, 2003, **93**, 6258.
21 R. Bergamaschini, J. Tersoff, Y. Tu, J. J. Zhang, G. Bauer and F. Montalenti, *Phys. Rev. Lett.*, 2012, **109**, 156101.
22 A. A. Stekolnikov and F. Bechstedt, *Phys. Rev. B: Condens. Matter Mater. Phys.*, 2005, **72**, 125326.
23 C. S. Lent, P. D. Tougaw, W. Porod and G. H. Bernstein, *Nanotechnology*, 1993, **4**, 49.